

RESEARCH ARTICLE

10.1002/2014JA020158

Key Points:

- Discrete emissions have smaller bandwidth and larger coherence coefficient
- Bandwidth increases with L , f_{pe}/f_{ce} , but decreases with density and coherence
- QL theory may be suitable for hiss-like waves but not for all discrete waves

Supporting Information:

- Readme
- Text S1
- Figure S1
- Figure S2
- Figure S3

Correspondence to:

X. Gao,
gaoxl@mail.ustc.edu.cn

Citation:

Gao, X., W. Li, R. M. Thorne, J. Bortnik, V. Angelopoulos, Q. Lu, X. Tao, and S. Wang (2014), Statistical results describing the bandwidth and coherence coefficient of whistler mode waves using THEMIS waveform data, *J. Geophys. Res. Space Physics*, 119, 8992–9003, doi:10.1002/2014JA020158.

Received 5 MAY 2014

Accepted 15 OCT 2014

Accepted article online 20 OCT 2014

Published online 20 NOV 2014

Statistical results describing the bandwidth and coherence coefficient of whistler mode waves using THEMIS waveform data

X. Gao^{1,2}, W. Li², R. M. Thorne², J. Bortnik², V. Angelopoulos³, Q. Lu¹, X. Tao¹, and S. Wang¹

¹CAS Key Laboratory of Geospace Environment, Department of Geophysics and Planetary Science, University of Science and Technology of China, Hefei, China, ²Department of Atmospheric and Oceanic Sciences, UCLA, Los Angeles, California, USA, ³Institute of Geophysics and Planetary Physics/Earth and Space Sciences, UCLA, Los Angeles, California, USA

Abstract The bandwidths and coherence coefficients of lower band whistler mode waves are analyzed using Time History of Events and Macroscale Interactions during Substorms (THEMIS) waveform data for rising tones, falling tones, and hiss-like emissions separately. We also evaluate their dependences on the spatial location, electron density, the ratio of plasma frequency to local electron gyrofrequency (f_{pe}/f_{ce}), and the wave amplitude. Our results show that the bandwidth normalized by the local electron gyrofrequency (f_{ce}) of rising and falling tones is very narrow ($\sim 0.01 f_{ce}$), smaller than that of the hiss-like emissions ($\sim 0.025 f_{ce}$). Meanwhile, the normalized bandwidth of discrete emissions gradually decreases with increasing wave amplitude, whereas that of hiss-like emissions increases slowly. The coherence coefficient of rising and falling tones is extremely large (~ 1), while the coherence coefficient of hiss-like emissions is smaller but is still larger than 0.5. For all categories of whistler mode waves, the normalized bandwidth increases at larger L shells. Furthermore, the normalized bandwidth is positively correlated with local f_{pe}/f_{ce} but is inversely correlated with the electron density. Interactions between radiation belt electrons and whistler mode waves have been widely described by quasi-linear diffusion theory. Our results suggest that although quasi-linear theory is not entirely applicable for modeling electron interactions with rising and falling tones due to their narrow bandwidth and high coherence coefficient, it is suitable to treat wave-particle interactions between electrons and low-amplitude hiss-like emissions. Moreover, the correlations between the normalized bandwidth of chorus waves (especially the discrete emissions) and other parameters may provide insights for the generation mechanism of chorus waves.

1. Introduction

Whistler mode waves are very common and intense electromagnetic emissions that occur in the inner magnetosphere, with a frequency range that generally extends from 0.1 to $0.8 f_{ce}$ (where the f_{ce} is the equatorial electron gyrofrequency) [Burtis and Helliwell, 1969; Tsurutani and Smith, 1974, 1977; Meredith et al., 2001; Li et al., 2012]. Typically, they are observed in two distinct frequency bands (lower band and upper band) with a minimum wave power near $0.5 f_{ce}$ [Tsurutani and Smith, 1974; Koons and Roeder, 1990]. Outside the plasmopause, whistler mode waves appear either as banded hiss-like emissions or as a series of discrete rising and falling tones [Santolik et al., 2009; Li et al., 2011b, 2012], but in some cases, the two kinds of emissions can coexist [Pope, 1963; Koons and Roeder, 1990; Santolik et al., 2009]. Chorus waves, which have a discrete structure, are excited through nonlinear resonant interactions with the energetic electrons (tens of keV) [Nunn, 1974; Omura et al., 2008, 2012; Li et al., 2010], although the details of the generation process are still under investigation. The main source region of chorus waves is in the vicinity of the geomagnetic equatorial plane [LeDocq et al., 1998; Lauben et al., 2002; Santolik et al., 2005; Li et al., 2009], while another possible source region is in the dayside outer zone [Tsurutani et al., 2009], where dayside off-equatorial minima of magnetic field strength occur when the terrestrial dipole magnetic field is compressed by the solar wind.

Whistler mode waves are very important in controlling the outer radiation belt dynamics due to their dual role in both the acceleration and precipitation of radiation belt energetic electrons [Horne et al., 2003; Bortnik and Thorne, 2007; Summers et al., 2007; Thorne, 2010]. There is considerable theoretical and observational evidence that chorus waves play a key role in transferring energy from the more abundant low-energy

electrons (tens of keV) to relativistic electrons through efficient energy diffusion [e.g., *Summers et al.*, 2002; *Horne et al.*, 2005; *Thorne et al.*, 2013]. This local acceleration of electrons by chorus waves is an important mechanism for the enhancements of energetic electron fluxes near the heart of the outer radiation belt during storms or prolonged periods of substorm activity [*Summers et al.*, 1998; *Meredith et al.*, 2001; *Horne et al.*, 2005; *Thorne et al.*, 2013]. These whistler mode waves can also scatter electrons into the loss cone leading to precipitation into the atmosphere [e.g., *Lorentzen et al.*, 2001; *Thorne et al.*, 2005; *Lam et al.*, 2010]. Furthermore, the electron pitch angle diffusion by chorus waves can lead to the formation of the pancake distributions typically observed in Earth's magnetosphere [*Meredith et al.*, 1999; *Su et al.*, 2009; *Tao et al.*, 2011] and provide a major source of energy for the diffuse and pulsating aurora [*Ni et al.*, 2008, 2011; *Nishimura et al.*, 2010, 2013; *Thorne et al.*, 2010].

Quasi-linear diffusion theory has commonly been used as a fundamental tool to model the effects of chorus waves on the energetic electrons [*Kennel and Engelman*, 1966; *Horne et al.*, 2003; *Thorne et al.*, 2010, 2013; *Ni et al.*, 2011a, 2011b]. The interactions between electrons and the broadband and low-amplitude whistler mode waves are well described with quasi-linear theory to determine the timescales for electron energy diffusion and pitch angle diffusion due to chorus waves [*Horne et al.*, 2003; *Ni et al.*, 2008; *Thorne et al.*, 2010]. Moreover, global models describing the long-term evolution of the radiation belt during geomagnetic storms or substorms have also been developed [e.g., *Albert et al.*, 2009; *Shprits et al.*, 2009; *Su et al.*, 2010; *Artemyev et al.*, 2012; *Tu et al.*, 2013; *Glauert et al.*, 2014], which is a crucial part of space weather prediction.

Nonlinear effects become important when the interaction between electrons and a large amplitude monochromatic whistler mode wave is considered. When the wave amplitude is large, the fundamental mode of electron scattering can switch from being stochastic to deterministic, which leads to phase bunching or phase trapping [e.g., *Inan et al.*, 1978; *Albert*, 2002; *Bortnik et al.*, 2008]. However, when the single wave is extended to a realistic whistler mode wave with modulated wave amplitudes, the electrons exhibit complicated motions caused by both quasi-linear and nonlinear interactions [*Tao et al.*, 2012, 2013]. Specifically, by comparing the diffusion coefficients obtained by quasi-linear theory and test particle simulation, *Tao et al.* [2012] found that there can be large differences when the wave amplitude is large and the bandwidth is narrow. In their study, for a wave bandwidth of $0.1 f_{ce}$ (also some other fixed parameters), quasi-linear theory was found to be reliable only when the wave amplitude was smaller than 0.1 nT ($B_w^2/B_0^2 \approx 2 \times 10^{-7}$) for 10 keV electrons and 0.66 nT ($B_w^2/B_0^2 \approx 7 \times 10^{-6}$) for 1 MeV electrons. Furthermore, recent observational results revealed that chorus waves with large amplitudes (>100 pT) often occurred [*Cattell et al.*, 2008; *Cully et al.*, 2008; *Wilson et al.*, 2011], especially during periods of increased geomagnetic activity [*Li et al.*, 2011a] or in the dayside outer zone [*Tsurutani et al.*, 2009]. Therefore, the nonlinear effect caused by discrete chorus emissions may also play an important role in the radiation belt electron dynamics, although its relative importance is still under debate.

Although the bandwidth of whistler mode waves is a key parameter in studying their interactions with electrons, comprehensive statistical information describing the bandwidth of whistler mode waves is very limited, probably due to the limited electric and magnetic wave data with high time resolution. Thanks to the THEMIS (Time History of Events and Macroscale Interactions during Substorms) mission [*Angelopoulos*, 2008], sufficient waveform data are now available to conduct such a study. By analyzing the waveform data collected from 1 June 2008 to 1 June 2013, we have investigated the global distribution of the bandwidth of lower band whistler mode waves including rising and falling tone chorus and hiss-like emissions and its dependence on the electron density, wave amplitude, and the ratio of plasma frequency to electron gyrofrequency. The coherence coefficient, which provides information on the distribution of wave vectors, is also evaluated in our paper. In section 2, we describe the analysis of the THEMIS wave data. The global distribution of whistler mode wave events and statistical results of their bandwidths and coherence coefficients are presented in section 3. In section 4, we summarize and further discuss our principal results.

2. THEMIS Wave Data Analysis

The THEMIS spacecraft, consisting of five identically instrumented probes (A, B, C, D, and E), operate in highly elliptical orbits with apogees above $10 R_E$ and perigees below $2 R_E$ [*Angelopoulos*, 2008], in the near-equatorial magnetosphere, and thus offer an excellent opportunity to study whistler mode waves. The whistler mode

emissions can be detected by the Search Coil Magnetometer (SCM) [Le Contel *et al.*, 2008; Roux *et al.*, 2008] and Electric Field Instrument (EFI) [Bonnell *et al.*, 2008]. SCM measures the magnetic fluctuations in three orthogonal directions, covering the frequency range from 0.1 Hz to 4 kHz. EFI captures waveforms in three orthogonal directions from DC (direct current) up to 8 kHz. Several waveform bursts, each lasting about 6–8 s, are recorded every day simultaneously from SCM and EFI with a sampling frequency up to ~16 kHz. The wave burst data (scw and efw files) recorded from three inner probes (A, D, and E) are analyzed in this study to obtain the polarization properties of the chorus waves. The fluxgate magnetometer (FGM) measures the background magnetic fields and their low-frequency fluctuations (up to 64 Hz) [Auster *et al.*, 2008]. FGM data in this study are utilized to evaluate local electron cyclotron frequencies in order to scale whistler mode wave frequencies. The plasma density inferred from the spacecraft potential and electron thermal speed [e.g., Li *et al.*, 2010] is used to differentiate whistler mode waves observed outside the plasmopause from plasmaspheric hiss using the same method as Li *et al.* [2010].

Following the procedure developed by Bortnik *et al.* [2007] (essentially an implementation of Means [1972]), we analyze the three components of magnetic fields (rotated into the field-aligned coordinate system) from wave burst data to obtain the polarization parameters of whistler mode waves. In the field-aligned coordinate system, z axis is along the direction of the background magnetic field, x axis is perpendicular to both the azimuthal vector in the solar magnetic coordinate and the background magnetic field, and y axis completes the right-hand coordinate system. These calculated wave polarization parameters have a time resolution of ~0.032 s, which is much smaller than the typical temporal duration of each discrete chorus element (a few tenths of seconds [Cully *et al.*, 2008; Santolik *et al.*, 2008; Macusova *et al.*, 2010; Li *et al.*, 2011b, 2012]). The polarization ratio (R_p), defined as the ratio of polarized power to total power, is used to evaluate the reliability of the other wave polarization parameters [Bortnik *et al.*, 2007]. The sense of the polarization is indicated by the sign of the ellipticity, which is >0 (<0) for right-hand (left-hand) rotation about the wave vector. Since whistler mode waves typically have a large polarization ratio and right-hand polarization, we only record the polarization parameters when $R_p > 0.9$ and ellipticity > 0.7 . Because only the magnetic fields are involved in this method, there is an inherent 180° ambiguity in the wave normal direction. Similar to Li *et al.* [2012], we also convert all the wave normal directions into values less than 90°. The coherence coefficient is given by $C_{ij}(\omega_0) = |\hat{S}_{ij}(\omega_0)|^2 / \hat{S}_{ii}(\omega_0)\hat{S}_{jj}(\omega_0)$ (where $\hat{S}_{ij}(\omega_0)$ is either the mean autopower spectrum ($i=j$) or the mean cross-power spectrum ($i \neq j$) and ω_0 is the angular wave frequency), using both the wave magnetic fields and electric fields from the waveform data following Lefeuvre and Parrot [1979]. The coherence coefficient can act as a qualitative measure of the distribution of wave vectors. When the coherence coefficient equals 1, the wave can be considered as a plane wave with a well-defined propagation direction. However, when the coherence coefficient is 0, the wave vectors are totally random and the wave can be treated as noise [Lefeuvre and Parrot, 1979].

3. Observational Results

The data set used in this study is collected from wave burst data from the three inner probes of THEMIS (A, D, and E), covering the main source region of chorus waves between 5 and 10 R_E at all magnetic local time (MLT). Since the THEMIS spacecraft are situated in near-equatorial orbits, the data samples are confined to low magnetic latitudes, typically less than $\pm 20^\circ$. The time period of the waveform data analyzed in the present study is from 1 June 2008 to 1 June 2013. The plasmaspheric hiss waves and other magnetosheath emissions are excluded in our database following the method of Li *et al.* [2010], and only the lower band whistler mode waves (0.1–0.5 f_{ce}) observed between the plasmopause and magnetopause are retained.

Whistler mode waves in the magnetosphere exhibit three kinds of structure in the frequency-time spectrogram, such as rising tones, falling tones, and hiss-like emissions. A representative example of rising tones is illustrated in Figure 1. Figure 1a shows a flag, which is used to identify whether the whistler mode emissions are rising tones (flag = 1), falling tones (flag = -1), or hiss-like emissions (flag = 0), and the flag is set to a NaN value if whistler mode waves are not detected. At each recording time, the frequency with the maximum magnetic spectral density is recorded after smoothing the adjacent three points. Then we calculate the frequency sweep rate using five adjacent points. If the sign of the frequency sweep rate remains positive (or negative) for longer than 0.1 s, the flag is set to 1 (or -1); otherwise, it is set to 0. This procedure is similar to that of Li *et al.* [2012]. Here we chose two perpendicular components of wave fields (E_y and B_x) to

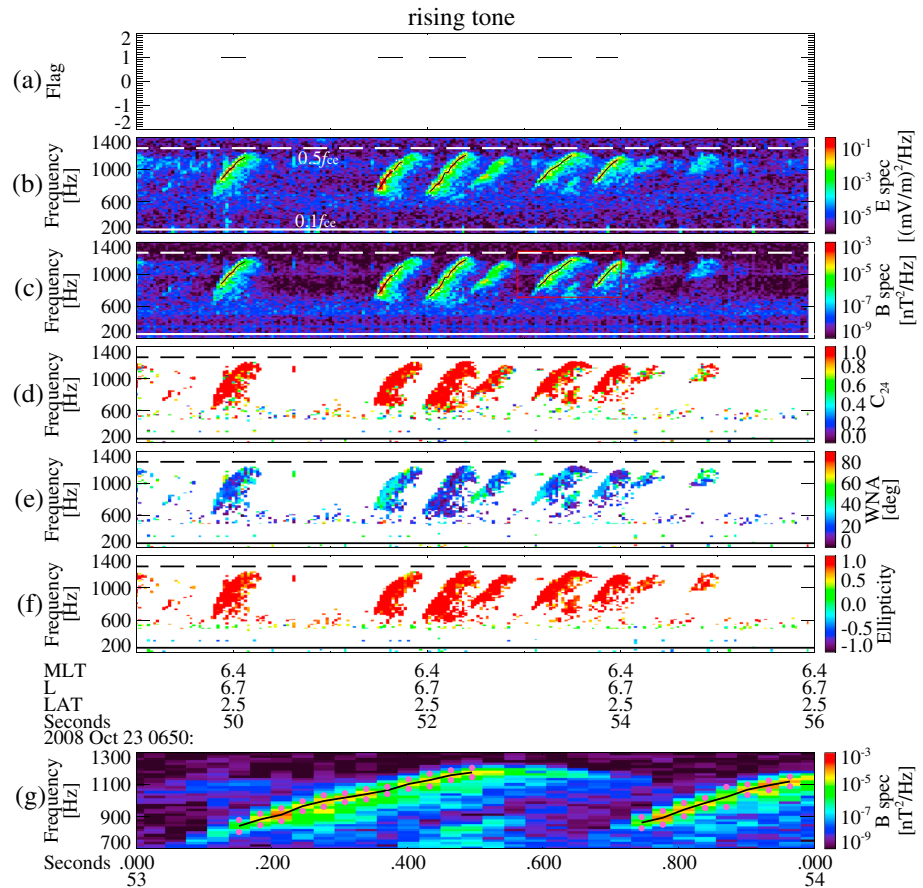


Figure 1. One wave event of rising tones observed by THEMIS D on 23 October 2008 showing (a) a flag which is used to classify the emission, (b) the frequency-time spectral density of wave electric field, (c) magnetic field, (d) coherence coefficient C_{24} , (e) wave normal angle (WNA), (f) ellipticity, and (g) expanded version of Figure 1c inside the red box. In Figures 1b–1f, the solid and dashed horizontal lines in white or black represent 0.1 and $0.5 f_{ce}$, respectively. In Figure 2g, the solid black line represents the peak frequency f_p obtained by Gaussian fitting at each time. The magenta points in Figure 1g denote the frequencies of $f_p \pm 2df'$ (where df' is the bandwidth at each time).

calculate the coherence coefficient (C_{24}), since the perpendicular components are always nonzero regardless of the wave normal angle. As shown in Figure 1d, the coherence coefficient C_{24} is nearly 1, which means that these rising tone emissions can be considered as being made up of a series of plane waves. This rising tone emission is nearly field aligned, with a wave normal angle smaller than 30° , as shown in Figure 1e. The right-hand polarization is clearly displayed in Figure 1f. Figure 1g is the expanded version of the magnetic frequency-time spectrogram inside the red box of Figure 1c. At each recording time, when the flag is equal to 1 (rising tone) or -1 (falling tone), we conduct a 21-point Gaussian fitting with the central frequency having the maximum magnetic spectral density to determine the peak frequency f_p and the bandwidth df (A full discussion regarding the definition, rationale, and artificial limitations of the bandwidth due to various signal processing effects is given in the supporting information). The employed Gaussian fitting function is $G(f) = A_0 \exp[-(f - f_p)^2/df^2] + C$, where A_0 and C are the peak magnetic spectral density and background noise, respectively. The peak frequencies are shown by black solid lines, and two other frequencies ($f_p \pm 2df'$) are represented by magenta points in Figure 1g. We find that the chorus element can well be identified by the magenta points, which indicates that the Gaussian fitting generally works well.

With the same pattern as Figure 1, Figure 2 shows a typical event consisting of falling tones. The falling tone has almost the same wave properties as the rising tone, except for the very oblique wave normal angle ($\sim 70^\circ$ shown in Figure 2e). The Gaussian fitting can also describe the falling tone element very well. One typical event of hiss-like emissions is presented in Figure 3. As shown in Figure 3e, this hiss-like emission is almost field aligned, with small wave normal angles. It is worth noting that the coherence coefficient of

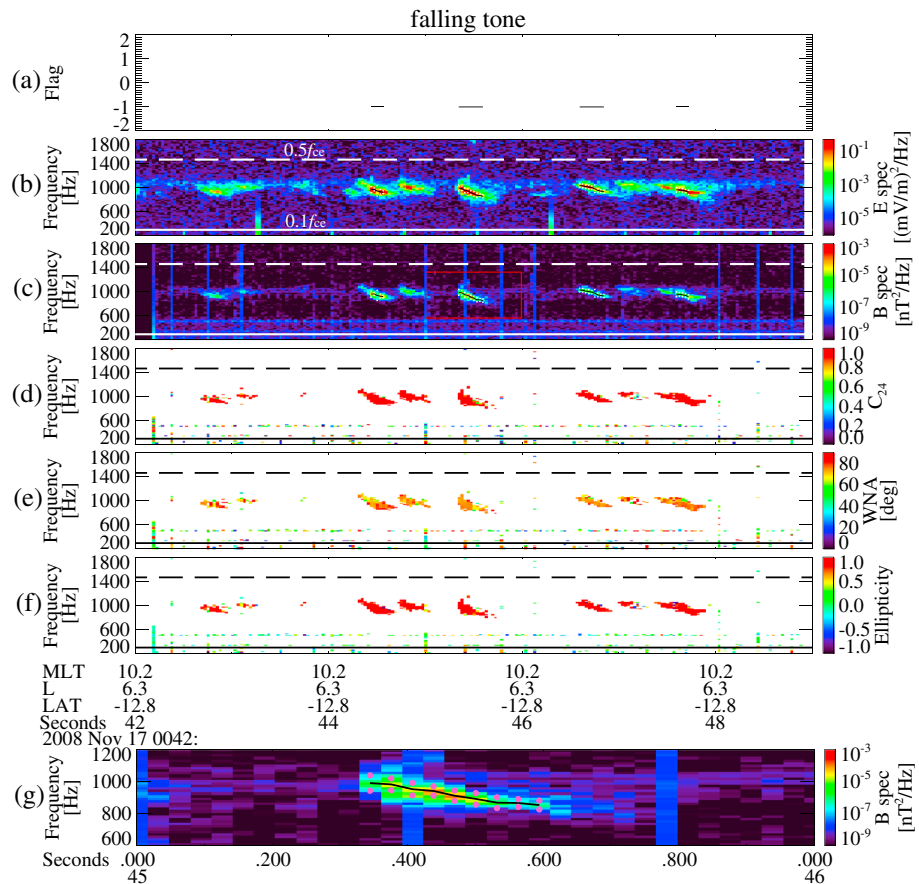


Figure 2. One wave event of falling tones observed by THEMIS E on 17 November 2008 displayed in the same format as Figure 1.

hiss-like emission is a little smaller compared to that of rising or falling tones but is still large (>0.5). This is quite different from plasmaspheric hiss, whose coherence coefficient is almost zero [Lefeuvre and Parrot, 1979]. For the hiss-like category, the Gaussian fitting at each recording time is performed by using all the points between 0.1 and $0.5 f_{ce}$ instead of 21 points. This is because the bandwidth of hiss-like emissions is larger than that of the rising or falling tones, as shown in section 3.2, and thus, it requires more points to be involved in the Gaussian fitting. Another two black dashed lines plotted in Figure 3g are at frequencies of $f_p \pm 2df$ (where df is the average of bandwidth df' over the entire event). Although the magenta points appear to be somewhat scattered, the black dashed lines representing the average bandwidths are quite consistent with the lower and upper cutoff of this banded hiss-like emission. Therefore, the Gaussian fitting generally works well for analyzing the local bandwidth of the hiss-like emissions. Another possible way to calculate the bandwidth of hiss-like emissions is to average the spectra over the entire event first, before performing the Gaussian fitting. The comparison of these two methods and relevant discussions are provided in the supporting information.

3.1. Global Distribution of Whistler Mode Wave Events

One wave burst is defined as one recording interval lasting about 6–8 s, similar to the examples shown in Figures 1–3. During one wave burst, if whistler mode waves are observed, this wave burst is called one wave event. All the wave events are classified into three categories according to the flag (Figures 1a–1f, 2a–2f, and 3a–3f), rising tones, falling tones, and hiss-like emissions, and a visual inspection is performed to confirm the validity of their categories. In our database, the total number of wave events for rising tones, falling tones, and hiss-like emissions is 1323, 186, and 1694 out of 12,400 wave bursts, respectively. For some wave events, in which both discrete (rising or falling tone) and hiss-like emissions coexist, we only regard them as the discrete (rising or falling tone) wave events, since the discrete emissions always have the predominant

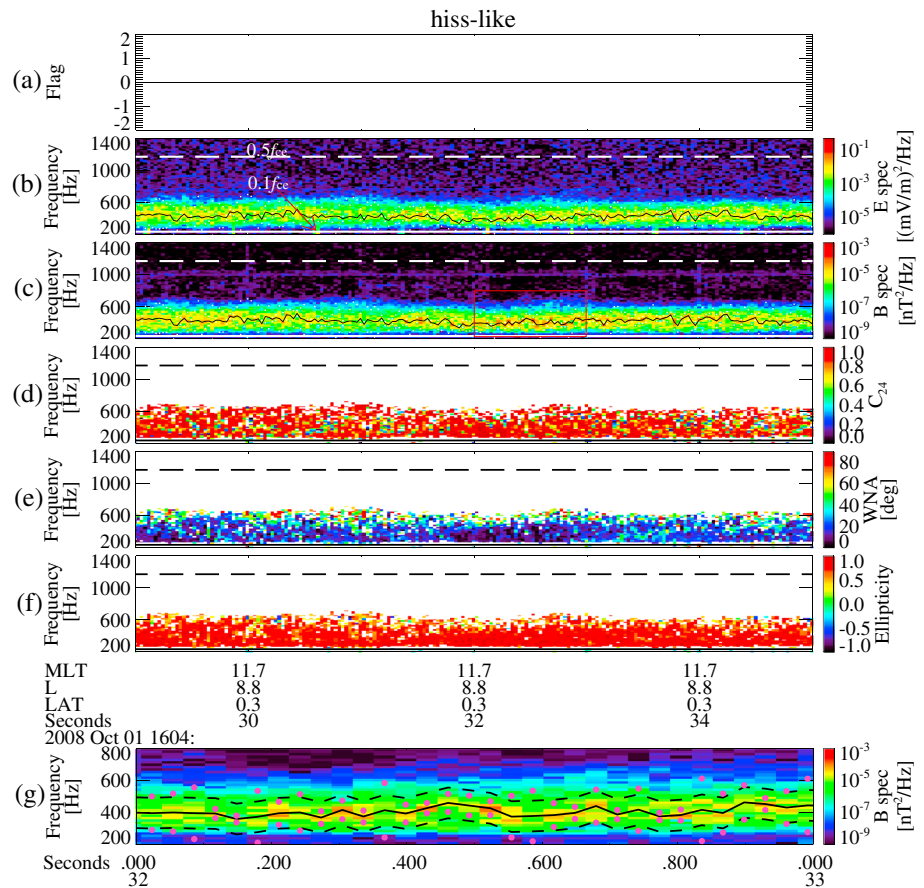


Figure 3. One wave event of hiss-like emissions observed by THEMIS A on 1 October 2008 displayed in the same format as Figures 1 and 2, except that in Figure 3g, where two dashed black lines represent the frequencies of $f_p \pm 2df'$ (where df' is the average bandwidth of the entire wave event).

magnetic spectral density. For one wave event, several important parameters are recorded at the recording time when its flag has a value (1, -1, or 0), including L shell, MLT, magnetic latitude (MLAT), bandwidth, coherence coefficient, wave amplitude (integrated over the frequency from 0.1 to $0.5 f_{ce}$), and electron density (inferred from the spacecraft potential according to Li *et al.* [2010]). Note that the flag is set to a NaN value if the recorded wave properties are not identified as either discrete rising/falling tones or hiss-like emissions. Subsequently, we averaged the recorded parameters to represent the values in each wave event, since the wave properties and plasma parameters over this short time period are normally very similar, as shown Figures 1–3. For the rising tone event shown in Figure 1 as an example, we calculated the above wave and plasma parameters by averaging the corresponding values for the data points with flag = 1.

Figures 4a and 4b show the global distribution of wave bursts in L-MLT and $|MLAT|$ -MLT regions. The color bar indicates the number of wave bursts in each bin, and the total number is about 12,400. The global distribution of wave events in L-MLT and $|MLAT|$ -MLT domains for three categories is displayed in Figures 4c–4h. Here the occurrence rate is defined as the ratio between the number of wave events in each bin and the number of wave bursts in the same bin. If the number of wave bursts in one bin is less than 10, this bin is discarded. From Figure 4a, we found that the coverage of waveform data is very limited on the nightside particularly at $<7 R_E$, and thus, the statistical significance in these regions may not be high. For rising tones, the high occurrence rate occurs at the low L shells from the predawn to the afternoon sector. However, the falling tones have the lowest occurrence rate with a preferential region from the predawn to the noon sector at low L shells. The hiss-like emissions have a very broad distribution in the L-MLT domain but have the extremely high occurrence rate from the predawn to the prenoon sector at relatively high L shells. In the $|MLAT|$ -MLT domain, all categories show an asymmetric distribution between dayside and nightside. Unlike the rising tones and hiss-like emissions,

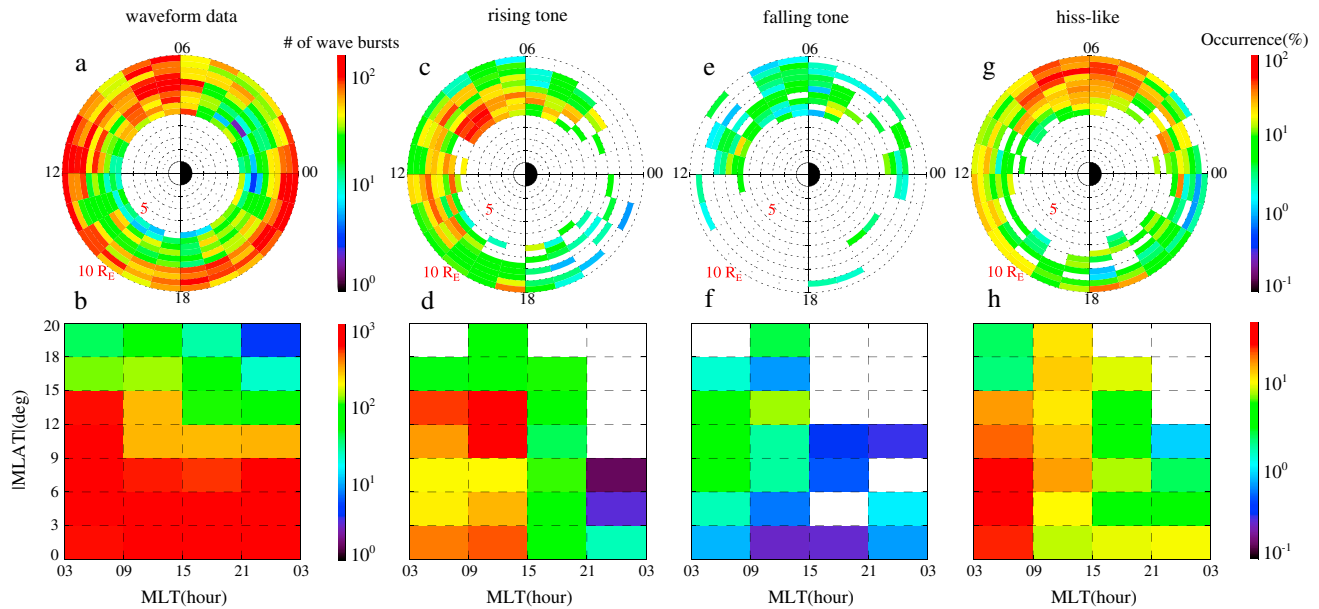


Figure 4. (a and b) The number of wave bursts, (c and d) relative occurrence rate of rising tones, (e and f) falling tones, and (g and h) hiss-like emissions in the L-MLT domain with a bin size of 0.5×1 MLT and $|MLAT|$ -MLT domain with a bin size of $3 \text{ MLAT} \times 6 \text{ MLT}$, respectively.

whose occurrence rate is higher at low magnetic latitudes, the falling tones are preferentially observed at slightly higher magnetic latitudes ($|MLAT| > 6^\circ$) on the dayside (Figure 4f). These statistical distributions of rising and falling tones and hiss-like emissions are generally consistent with *Li et al.* [2012], who analyzed their characteristics for a shorter time period from June 2008 to May 2012.

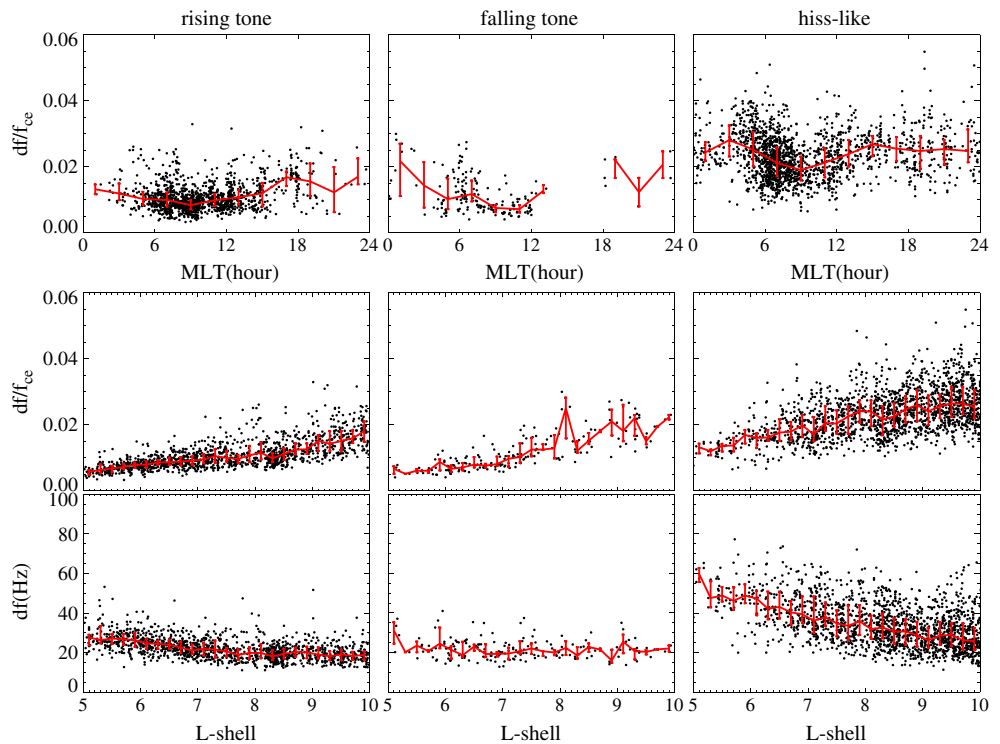


Figure 5. The normalized bandwidth df/f_{ce} as a function of (top row) MLT and (middle row) L shell, and (bottom row) the absolute bandwidth df as a function of L shell for rising tones, falling tones, and hiss-like emissions, respectively. The red lines represent the median values, with the first and third quartiles shown in vertical red bars.

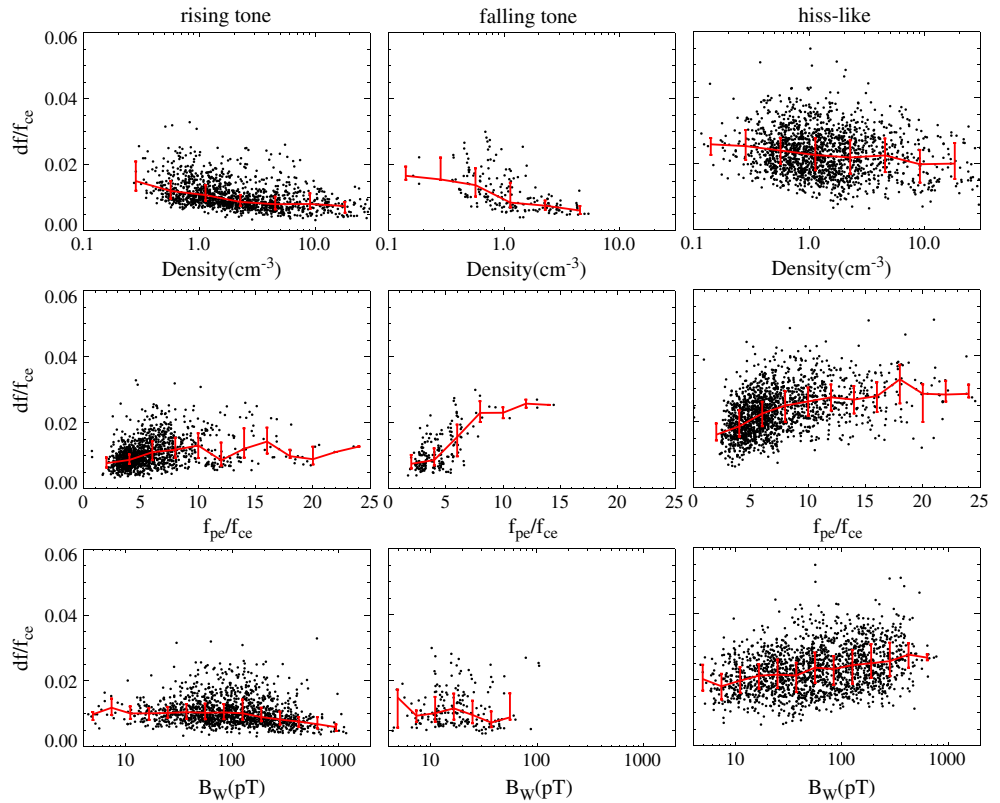


Figure 6. The normalized bandwidth df/f_{ce} as a function of (top row) electron density, (middle row) the ratio of plasma frequency to electron gyrofrequency f_{pe}/f_{ce} , and (bottom row) the wave amplitude B_W for rising tones, falling tones, and hiss-like emissions, respectively. The red lines represent the median values, with the first and third quartiles shown as vertical red bars.

3.2. Bandwidth of Whistler Mode Waves

The bandwidth df shown in this subsection is the average of bandwidth df' over the entire wave event with the designated flag value as mentioned above. Figure 5 shows the normalized bandwidth df/f_{ce} as a function of MLT and L shell and the absolute bandwidth df as a function of L shell for the three categories, respectively. Each black dot represents a wave event in its corresponding category, and the median values are denoted by red lines with the first and third quartiles as vertical red bars. For all the categories, the normalized bandwidth is nearly independent of MLT as shown in Figure 5 (top row). However, a weak minimum of bandwidths at ~ 9 MLT is found for all categories. In the middle row, there is a very clear trend for the normalized bandwidth to increase with L shells. Furthermore, the slopes for the three categories are almost the same (~ 0.003). In the bottom row, the absolute bandwidth df for the three categories gradually decreases with the L shell. Therefore, the increasing trend of the normalized bandwidth with L shell is probably mainly caused by the decrease of the ambient magnetic field. Overall, the discrete chorus waves (rising and falling tones) have a narrower normalized bandwidth (~ 0.01) compared to the hiss-like emissions (~ 0.025).

The dependences of the normalized bandwidth df/f_{ce} on the electron density, the ratio of plasma frequency to local electron gyrofrequency f_{pe}/f_{ce} , and the wave amplitude B_W for the three categories are demonstrated in Figure 6. As the electron density increases, the bandwidth df/f_{ce} decreases for all the categories (Figure 6, top row). This correlation is quite consistent with the dependence of the normalized bandwidth on L shell, since the electron density is generally inversely correlated with the L shell. Both the discrete (rising and falling tone) and hiss-like emissions have narrower bandwidths df/f_{ce} in the region with lower values of f_{pe}/f_{ce} (Figure 6, middle row). Furthermore, the majority of discrete emissions (rising and falling tones) occur in the region with low values of f_{pe}/f_{ce} (< 8), while a large portion of the hiss-like emissions is observed in the region with large values of f_{pe}/f_{ce} (> 8). This is consistent with the previous work by Li *et al.* [2012].

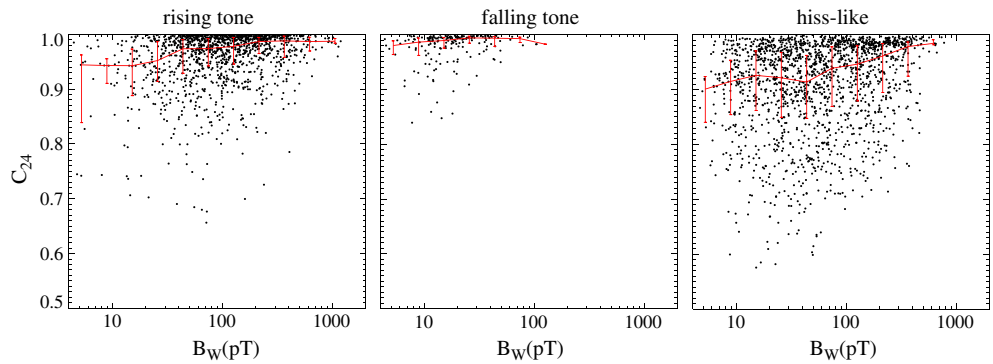


Figure 7. The dependences of coherence coefficient C_{24} on the wave amplitude B_W for rising tones, falling tones, and hiss-like emissions, respectively. The red lines represent the median values, with the first and third quartiles as vertical red bars.

The dependence of the normalized bandwidth on the wave amplitude is quite different between the discrete and hiss-like emissions (Figure 6, bottom row). For the hiss-like emissions, the normalized bandwidth gradually increases with the increase of the wave amplitude. However, with the increase of the wave amplitude, the normalized bandwidth of discrete emissions decreases slowly especially for the rising tones, although this trend is not very clear. The physics underlying the opposite correlations of the bandwidth of discrete and hiss-like emissions with the wave amplitude might be related to their different generation mechanisms, but further investigation is needed to explain it, which is beyond the scope of this paper.

3.3. Coherence Coefficient of Whistler Mode Waves

The coherence coefficient C_{24} discussed here is also the average of the coherence coefficient over the whole wave event with the designated flag value, similar to the bandwidth df . Figure 7 shows the coherence coefficient C_{24} as a function of the wave amplitude B_w for the three wave categories. First, for all the categories C_{24} , the coherence coefficient increases with the increasing wave amplitude. Second, for the rising and falling tones, the coherence coefficient is very large, nearly equal to 1. Third, the coherence coefficient of hiss-like emissions is smaller compared to that of discrete emissions but is still larger than 0.5. Therefore, some of the hiss-like emissions cannot be simply treated as a plane wave with a well-defined propagation direction but better with a distribution function of wave vectors. This is essentially different from the case of plasmaspheric hiss waves, whose wave vectors are more likely to be random and coherence coefficient is almost zero [Lefeuvre and Parrot, 1979]. The correlation between the coherence coefficient C_{24} and the normalized bandwidth df/f_{ce} is also shown in Figure 8 for the three wave categories. For both the discrete and hiss-like emissions, as the coherence coefficient increases, the normalized bandwidth becomes smaller, but the trend for hiss-like emissions is a little weaker.

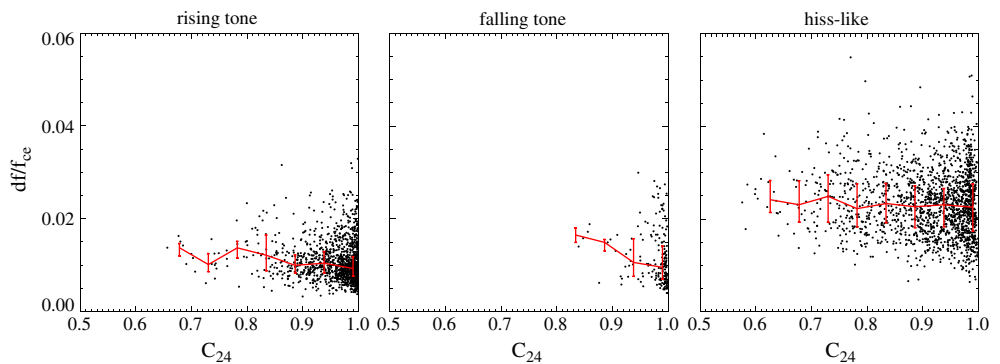


Figure 8. The correlation between the normalized bandwidth df/f_{ce} and the coherence coefficient C_{24} for rising tones, falling tones, and hiss-like emissions, respectively. The red lines represent the median values, with the first and third quartiles as vertical red bars.

4. Summary and Discussion

We have utilized the multiyear waveform data from the three inner THEMIS spacecraft to evaluate the bandwidth and coherence coefficient of whistler mode waves and their dependences on wave amplitude, electron density, and the ratio of plasma frequency to local electron gyrofrequency. This comprehensive analysis is performed for three different categories of whistler mode emissions, rising tones, falling tones, and hiss-like emissions separately. The principal results are summarized as follows:

1. The rising and falling tones preferentially occur at $L < 8$ and regions where $f_{pe}/f_{ce} < 8$, whereas the hiss-like emissions are dominant at $L > 7$ and regions where f_{pe}/f_{ce} is in the range 2–15.
2. The bandwidth of the rising and falling tone is about $0.01 f_{ce}$, smaller than that of the hiss-like emission ($\sim 0.025 f_{ce}$). The normalized bandwidth df/f_{ce} for the discrete and hiss-like emissions increases with increasing L , with a slope of ~ 0.003 . However, the absolute bandwidth df gradually decreases with increasing L . Furthermore, the normalized bandwidth is positively related to the f_{pe}/f_{ce} but is inversely correlated with the electron density. With the increase of the wave amplitude, the bandwidth df/f_{ce} of the discrete emission gradually decreases, whereas the bandwidth df/f_{ce} of the hiss-like emission increases slowly.
3. The coherence coefficient of the rising and falling tones is large (~ 1), while the coherence coefficient of the hiss-like emission is smaller but is still larger than 0.5. For all the three categories, with the increase of the wave amplitude, the coherence coefficient becomes larger. Moreover, we also find the inverse correlation between the normalized bandwidth and the coherence coefficient.

It is important to note that the wave bandwidth defined in the present paper is different from the long-run bandwidth, which is typically used to model the whistler mode wave spectrum when simulating energetic electron dynamics caused by chorus wave scattering in diffusion-based simulations [e.g., *Horne et al.*, 2005; *Li et al.*, 2007; *Su et al.*, 2009]. The bandwidth defined in our study is used to describe the wave bandwidth (based on a Gaussian fitting) inside a wave element within $< \sim 0.1$ s, whereas the bandwidth used to model whistler mode wave spectrum is obtained by averaging the wave spectrum over many chorus elements (more than a few seconds). Since it is the bandwidth inside each element, which determines the mode of electron scattering (i.e., stochastic or deterministic) occurring within < 0.1 s [e.g., *Bortnik et al.*, 2008], we quantitatively and statistically evaluated the bandwidth inside each element for three types of whistler mode wave emissions (rising tones, falling tones, and hiss-like emissions). We note that for rising and falling tones, due to the finite fast Fourier transform (FFT) window size and frequency sweep rate, the calculated bandwidths could be affected by the drift frequency and frequency resolution. Therefore, in this survey, we carefully chose the time step of the FFT window (~ 0.032 s) to ensure the optimum resolution in both time and frequency, which limits the artificial effect to an insignificant level (two test studies supporting this optimum time step are shown in the supporting information). Furthermore, the dependences of the normalized bandwidth on the ratio of plasma frequency to electron gyrofrequency shown from our results may also provide some constraints for the generation mechanisms of whistler mode waves, which is beyond the scope of this paper and needs further investigation.

There have been considerable works done on the pitch angle scattering of radiation belt electrons by chorus waves using quasi-linear theory [*Horne et al.*, 2003; *Li et al.*, 2007; *Albert et al.*, 2009; *Ni et al.*, 2008, 2011a, 2011b; *Shprits et al.*, 2009; *Thorne et al.*, 2010; *Glauert et al.*, 2014; *Tu et al.*, 2014]. Most of these works, however, have addressed the problem of electron diffusion based on the assumption of broadband and small-amplitude whistler mode chorus waves. The most important and fundamental idea in quasi-linear theory is that electrons interact with the wave fields through the cyclotron resonance along their trajectories and experience a series of scattering that is random in both direction and strength [*Kennel and Engelman*, 1966]. Therefore, the electrons undergo a random walk in pitch angle space, and the diffusion of the whole population can be achieved. According to our results, the bandwidth of discrete emissions is very narrow, and even narrower when the wave amplitude is larger. Furthermore, their coherence coefficients are extremely high, nearly one. The physics is fundamentally different when it involves highly coherent narrowband whistler mode waves. When the electrons encounter such waves, the series of scattering experienced by the particles is not completely random in direction or strength [*Inan et al.*, 1978; *Albert*, 2002; *Bortnik et al.*, 2008]. The electrons can be phase locked with the wave for a while and undergo large net pitch angle changes in a single encounter with the wave [*Bortnik et al.*, 2008; *Tao et al.*, 2012]. It is therefore not entirely correct to

assume that the trapped electrons execute a random walk in pitch angle during the course of one bounce period when interacting with narrowband chorus waves. However, the situation may be different for hiss-like emissions. They have larger bandwidths than the discrete emissions, and the small bandwidth of hiss-like emissions preferentially occurs when the wave amplitude is small. Therefore, quasi-linear theory may still perform well when it only involves the hiss-like emissions except for few events with relatively narrower bandwidth ($<0.02 f_{ce}$) and very large amplitude (>0.5 nT).

Acknowledgments

The work at UCLA was supported by NASA grants NNX11AD75G, NNX11AR64G, NNX12AD12G, NNX13AI61G, and NSF grant AGS 1405054. This work was also supported by the National Science Foundation of China, Grant 41274124, 41274144, 973 Program (2012CB825602). The authors acknowledge A. Roux and O. LeContel for use of SCM data, J. W. Bonnell and F. S. Mozer for use of EFI data, and K. H. Glassmeier, U. Auster, and W. Baumjohann for the use of FGM data provided under the lead of the Technical University of Braunschweig and with financial support through the German Ministry for Economy and Technology and the German Center for Aviation and Space (DLR) under contract 50 OC 0302. We acknowledge the THEMIS data used in this study obtained from <http://themis.ssl.berkeley.edu/data/themis/>.

Michael Liemohn thanks the reviewers for their assistance in evaluating the paper.

References

- Albert, J. (2002), Nonlinear interaction of outer zone electrons with VLF waves, *Geophys. Res. Lett.*, *29*(8), 1275, doi:10.1029/2001GL013941.
- Albert, J. M., N. P. Meredith, and R. B. Horne (2009), Three-dimensional diffusion simulation of outer radiation belt electrons during the 9 October 1990 magnetic storm, *J. Geophys. Res.*, *114*, A09214, doi:10.1029/2009JA014336.
- Angelopoulos, V. (2008), The THEMIS mission, *Space Sci. Rev.*, *141*(1–4), 5–34, doi:10.1007/s11214-008-9336-1.
- Artemyev, A., O. Agapitov, V. Krasnoselskikh, H. Breuillard, and G. Rolland (2012), Statistical model of electron pitch angle diffusion in the outer radiation belt, *J. Geophys. Res.*, *117*, A08219, doi:10.1029/2012JA017826.
- Auster, H. U., et al. (2008), The THEMIS fluxgate magnetometer, *Space Sci. Rev.*, *141*(1–4), 235–264, doi:10.1007/s11214-008-9365-9.
- Bonnell, J. W., F. S. Mozer, G. T. Delory, A. J. Hull, R. E. Ergun, C. M. Cully, V. Angelopoulos, and P. R. Harvey (2008), The Electric Field Instrument (EFI) for THEMIS, *Space Sci. Rev.*, *141*(1–4), 303–341, doi:10.1007/s11214-008-9469-2.
- Bortnik, J., and R. M. Thorne (2007), The dual role of ELF/VLF chorus waves in the acceleration and precipitation of radiation belt electrons, *J. Atmos. Sol. Terr. Phys.*, *69*, 378–386, doi:10.1016/j.jastp.2006.05.030.
- Bortnik, J., J. W. Cutler, C. Dunson, and T. E. Bleier (2007), An automatic wave detection algorithm applied to Pc1 pulsations, *J. Geophys. Res.*, *112*, A04204, doi:10.1029/2006JA011900.
- Bortnik, J., R. M. Thorne, and U. S. Inan (2008), Nonlinear interaction of energetic electrons with large amplitude chorus, *Geophys. Res. Lett.*, *35*, L21102, doi:10.1029/2008GL035500.
- Burtis, W. J., and R. A. Helliwell (1969), Banded chorus—A new type of VLF radiation observed in the magnetosphere by OGO 1 and OGO 3, *J. Geophys. Res.*, *74*(11), 3002–3010, doi:10.1029/JA074i011p03002.
- Cattell, C., et al. (2008), Discovery of very large amplitude whistler mode waves in Earth's radiation belts, *Geophys. Res. Lett.*, *35*, L01105, doi:10.1029/2007GL032009.
- Cully, C. M., J. W. Bonnell, and R. E. Ergun (2008), THEMIS observations of long-lived regions of large-amplitude whistler waves in the inner magnetosphere, *Geophys. Res. Lett.*, *35*, L17516, doi:10.1029/2008GL033643.
- Glauert, S. A., R. B. Horne, and N. P. Meredith (2014), Three-dimensional electron radiation belt simulations using the BAS Radiation Belt Model with new diffusion models for chorus, plasmaspheric hiss, and lightning-generated whistlers, *J. Geophys. Res. Space Physics*, *119*, 268–289, doi:10.1002/2013JA019281.
- Horne, R. B., S. A. Glauert, and R. M. Thorne (2003), Resonant diffusion of radiation belt electrons by whistler mode chorus, *Geophys. Res. Lett.*, *30*(9), 1493, doi:10.1029/2003GL016963.
- Horne, R. B., R. M. Thorne, S. A. Glauert, J. M. Albert, N. P. Meredith, and R. R. Anderson (2005), Timescale for radiation belt electron acceleration by whistler mode chorus waves, *J. Geophys. Res.*, *110*, A03225, doi:10.1029/2004JA010811.
- Inan, U. S., T. F. Bell, and R. A. Helliwell (1978), Nonlinear pitch angle scattering of energetic electrons by coherent VLF waves in the magnetosphere, *J. Geophys. Res.*, *83*(A7), 3235–3253, doi:10.1029/JA083iA07p03235.
- Kennel, C. F., and F. Engelman (1966), Velocity space diffusion from weak plasma turbulence in a magnetic field, *Phys. Fluids*, *9*(12), 2377, doi:10.1063/1.1761629.
- Koons, H. C., and J. L. Roeder (1990), A survey of equatorial magnetospheric wave activity between 5 and 8 R_E , *Planet. Space Sci.*, *38*(10), 1335–1341, doi:10.1016/0032-0633(90)90136-E.
- Lam, M. M., R. B. Horne, N. P. Meredith, S. A. Glauert, T. Moffat-Griffin, and J. C. Green (2010), Origin of energetic electron precipitation >30 keV into the atmosphere, *J. Geophys. Res.*, *115*, A00F08, doi:10.1029/2009JA014619.
- Lauben, D. S., U. S. Inan, T. F. Bell, and D. A. Gurnett (2002), Source characteristics of ELF/VLF chorus, *J. Geophys. Res.*, *107*(A12), 1429, doi:10.1029/2000JA003019.
- Le Contel, O., et al. (2008), First results of the THEMIS search coil magnetometers, *Space Sci. Rev.*, *141*, 509–534, doi:10.1007/s11214-008-9371-y.
- LeDocq, M. J., D. A. Gurnett, and G. B. Hospodarsky (1998), Chorus source locations from VLF Poynting flux measurements with the Polar spacecraft, *Geophys. Res. Lett.*, *25*(21), 4063–4066, doi:10.1029/1998GL900071.
- Lefevre, F., and M. Parrot (1979), Use of the coherence function for the automatic recognition of chorus and hiss observed by Geos, *J. Atmos. Terr. Phys.*, *41*(2), 143–152, doi:10.1016/0021-9169(79)90006-0.
- Li, W., Y. Y. Shprits, and R. M. Thorne (2007), Dynamic evolution of energetic outer zone electrons due to wave-particle interactions during storms, *J. Geophys. Res.*, *112*, A10220, doi:10.1029/2007JA012368.
- Li, W., R. M. Thorne, V. Angelopoulos, J. Bortnik, C. M. Cully, B. Ni, O. LeContel, A. Roux, U. Auster, and W. Magnes (2009), Global distribution of whistler mode chorus waves observed on the THEMIS spacecraft, *Geophys. Res. Lett.*, *36*, L09104, doi:10.1029/2009GL037595.
- Li, W., et al. (2010), THEMIS analysis of observed equatorial electron distributions responsible for the chorus excitation, *J. Geophys. Res.*, *115*, A00F11, doi:10.1029/2009JA014845.
- Li, W., J. Bortnik, R. M. Thorne, and V. Angelopoulos (2011a), Global distribution of wave amplitudes and wave normal angles of chorus waves using THEMIS wave observations, *J. Geophys. Res.*, *116*, A12205, doi:10.1029/2011JA017035.
- Li, W., R. M. Thorne, J. Bortnik, Y. Y. Shprits, Y. Nishimura, V. Angelopoulos, C. Chaston, O. Le Contel, and J. W. Bonnell (2011b), Typical properties of rising and falling tone chorus waves, *Geophys. Res. Lett.*, *38*, L14103, doi:10.1029/2011GL047925.
- Li, W., R. M. Thorne, J. Bortnik, X. Tao, and V. Angelopoulos (2012), Characteristics of hiss-like and discrete whistler mode emissions, *Geophys. Res. Lett.*, *39*, L18106, doi:10.1029/2012GL053206.
- Lorentzen, K. R., J. B. Blake, U. S. Inan, and J. Bortnik (2001), Observations of relativistic electron microbursts in association with VLF chorus, *J. Geophys. Res.*, *106*(A4), 6017–6027, doi:10.1029/2000JA003018.
- Macusova, E., et al. (2010), Observations of the relationship between frequency sweep rates of chorus wave packets and plasma density, *J. Geophys. Res.*, *115*, A12257, doi:10.1029/2010JA015468.

- Means, J. D. (1972), Use of three-dimensional covariance matrix in analyzing polarization properties of plane waves, *J. Geophys. Res.*, *77*(28), 5551–5559, doi:10.1029/JA077i028p05551.
- Meredith, N. P., A. D. Johnstone, S. Szita, R. B. Horne, and R. R. Anderson (1999), "Pancake" electron distributions in the outer radiation belts, *J. Geophys. Res.*, *104*(A6), 12,431–12,444, doi:10.1029/1998JA900083.
- Meredith, N. P., R. B. Horne, and R. R. Anderson (2001), Substorm dependence of chorus amplitudes: Implications for the acceleration of electrons to relativistic energies, *J. Geophys. Res.*, *106*(A7), 13,165–13,178, doi:10.1029/2000JA900156.
- Ni, B. B., R. M. Thorne, Y. Y. Shprits, and J. Bortnik (2008), Resonant scattering of plasma sheet electrons by whistler mode chorus: Contribution to diffuse auroral precipitation, *Geophys. Res. Lett.*, *35*, L11106, doi:10.1029/2008GL034032.
- Ni, B. B., R. M. Thorne, N. P. Meredith, R. B. Horne, and Y. Y. Shprits (2011a), Resonant scattering of plasma sheet electrons leading to diffuse auroral precipitation: 2. Evaluation for whistler mode chorus waves, *J. Geophys. Res.*, *116*, A04219, doi:10.1029/2010JA016233.
- Ni, B. B., R. M. Thorne, Y. Y. Shprits, K. G. Orlova, and N. P. Meredith (2011b), Chorus-driven resonant scattering of diffuse auroral electrons in nondipolar magnetic fields, *J. Geophys. Res.*, *116*, A06225, doi:10.1029/2011JA016453.
- Nishimura, Y., et al. (2010), Identifying the driver of pulsating aurora, *Science*, *330*(6000), 81–84, doi:10.1126/science.1193186.
- Nishimura, Y., et al. (2013), Structures of dayside whistler mode waves deduced from conjugate diffuse aurora, *J. Geophys. Res. Space Physics*, *118*, 664–673, doi:10.1029/2012JA018242.
- Nunn, D. (1974), Self-consistent theory of triggered VLF emissions, *Planet. Space Sci.*, *22*(3), 349–378, doi:10.1016/0032-0633(74)90070-1.
- Omura, Y., Y. Katoh, and D. Summers (2008), Theory and simulation of the generation of whistler mode chorus, *J. Geophys. Res.*, *113*, A04223, doi:10.1029/2007JA012622.
- Omura, Y., D. Nunn, and D. Summers (2012), Generation processes of whistler mode chorus emissions: Current status of nonlinear wave growth theory, in *Dynamics of the Earth's Radiation Belts and Inner Magnetosphere*, *Geophys. Monogr. Ser.*, vol. 199, edited by D. Summers et al., pp. 243–254, AGU, Washington, D. C., doi:10.1029/2012GM001347.
- Pope, J. H. (1963), A high-latitude investigation of natural very-low-frequency electromagnetic radiation known as chorus, *J. Geophys. Res.*, *68*(1), 83–99, doi:10.1029/JZ068i001p00083.
- Roux, A., O. Le Contel, C. Coillot, A. Bouabdellah, B. de la Porte, D. Alison, S. Ruocco, and M. C. Vassal (2008), The search coil magnetometer for THEMIS, *Space Sci. Rev.*, *141*(1–4), 265–275, doi:10.1007/s11214-008-9455-8.
- Santolik, O., D. A. Gurnett, J. S. Pickett, M. Parrot, and N. Cornilleau-Wehrlin (2005), Central position of the source region of storm-time chorus, *Planet. Space Sci.*, *53*, 299–305, doi:10.1016/j.pss.2004.09.056.
- Santolik, O., E. Macusova, E. E. Titova, B. V. Kozelov, D. A. Gurnett, J. S. Pickett, V. Y. Trakhtengerts, and A. G. Demekhov (2008), Frequencies of wave packets of whistler mode chorus inside its source region: A case study, *Ann. Geophys.*, *26*(6), 1665–1670.
- Santolik, O., D. A. Gurnett, J. S. Pickett, J. Chum, and N. Cornilleau-Wehrlin (2009), Oblique propagation of whistler mode waves in the chorus source region, *J. Geophys. Res.*, *114*, A00f03, doi:10.1029/2009JA014586.
- Shprits, Y. Y., D. Subbotin, and B. Ni (2009), Evolution of electron fluxes in the outer radiation belt computed with the VERB code, *J. Geophys. Res.*, *114*, A11209, doi:10.1029/2008JA013784.
- Su, Z. P., H. N. Zheng, and S. Wang (2009), Evolution of electron pitch angle distribution due to interactions with whistler mode chorus following substorm injections, *J. Geophys. Res.*, *114*, A08202, doi:10.1029/2009JA014269.
- Su, Z., F. Xiao, H. Zheng, and S. Wang (2010), STEERB: A three-dimensional code for storm-time evolution of electron radiation belt, *J. Geophys. Res.*, *115*, A09208, doi:10.1029/2009JA015210.
- Summers, D., R. M. Thorne, and F. L. Xiao (1998), Relativistic theory of wave-particle resonant diffusion with application to electron acceleration in the magnetosphere, *J. Geophys. Res.*, *103*(A9), 20,487–20,500, doi:10.1029/98JA01740.
- Summers, D., C. Ma, N. P. Meredith, R. B. Horne, R. M. Thorne, D. Heynderickx, and R. R. Anderson (2002), Model of the energization of outer-zone electrons by whistler mode chorus during the October 9, 1990 geomagnetic storm, *Geophys. Res. Lett.*, *29*(24), 2174, doi:10.1029/2002GL016039.
- Summers, D., B. Ni, and N. P. Meredith (2007), Timescales for radiation belt electron acceleration and loss due to resonant wave-particle interactions: 2. Evaluation for VLF chorus, ELF hiss, and electromagnetic ion cyclotron waves, *J. Geophys. Res.*, *112*, A04207, doi:10.1029/2006JA011993.
- Tao, X., R. M. Thorne, W. Li, B. Ni, N. P. Meredith, and R. B. Horne (2011), Evolution of electron pitch-angle distributions following injection from the plasma sheet, *J. Geophys. Res.*, *116*, A04229, doi:10.1029/2010JA016245.
- Tao, X., J. Bortnik, J. M. Albert, and R. M. Thorne (2012), Comparison of bounce-averaged quasi-linear diffusion coefficients for parallel propagating whistler mode waves with test particle simulations, *J. Geophys. Res.*, *117*, A10205, doi:10.1029/2012JA017931.
- Tao, X., J. Bortnik, J. M. Albert, R. M. Thorne, and W. Li (2013), The importance of amplitude modulation in nonlinear interactions between electrons and large amplitude whistler waves, *J. Atmos. Sol. Terr. Phys.*, *99*, 67–72, doi:10.1016/j.jastp.2012.05.012.
- Thorne, R. M. (2010), Radiation belt dynamics: The importance of wave-particle interactions, *Geophys. Res. Lett.*, *37*, L22107, doi:10.1029/2010GL044990.
- Thorne, R. M., T. P. O'Brien, Y. Y. Shprits, D. Summers, and R. B. Horne (2005), Timescale for MeV electron microburst loss during geomagnetic storms, *J. Geophys. Res.*, *110*, A09202, doi:10.1029/2004JA010882.
- Thorne, R. M., B. B. Ni, X. Tao, R. B. Horne, and N. P. Meredith (2010), Scattering by chorus waves as the dominant cause of diffuse auroral precipitation, *Nature*, *467*(7318), 943–946, doi:10.1038/Nature09467.
- Thorne, R. M., et al. (2013), Rapid local acceleration of relativistic radiation-belt electrons by magnetospheric chorus, *Nature*, *504*(7480), 411, doi:10.1038/Nature12889.
- Tsurutani, B. T., and E. J. Smith (1974), Postmidnight chorus: A substorm phenomenon, *J. Geophys. Res.*, *79*(1), 118–127, doi:10.1029/JA079i001p00118.
- Tsurutani, B. T., and E. J. Smith (1977), Two types of magnetospheric ELF chorus and their substorm dependences, *J. Geophys. Res.*, *82*(32), 5112–5128, doi:10.1029/JA082i032p05112.
- Tsurutani, B. T., O. P. Verkhoglyadova, G. S. Lakhina, and S. Yagitani (2009), Properties of dayside outer zone chorus during HILDCAA events: Loss of energetic electrons, *J. Geophys. Res.*, *114*, A03207, doi:10.1029/2008JA013353.
- Tu, W., G. S. Cunningham, Y. Chen, M. G. Henderson, E. Camporeale, and G. D. Reeves (2013), Modeling radiation belt electron dynamics during GEM challenge intervals with the DREAM3D diffusion model, *J. Geophys. Res. Space Physics*, *118*, 6197–6211, doi:10.1002/jgra.50560.
- Tu, W., G. S. Cunningham, Y. Chen, S. K. Morley, G. D. Reeves, J. B. Blake, D. N. Baker, and H. Spence (2014), Event-specific chorus wave and electron seed population models in DREAM3D using the Van Allen Probes, *Geophys. Res. Lett.*, *41*, 1359–1366, doi:10.1002/2013GL058819.
- Wilson, L. B., III, C. A. Cattell, P. J. Kellogg, J. R. Wygant, K. Goetz, A. Breneman, and K. Kersten (2011), The properties of large amplitude whistler mode waves in the magnetosphere: Propagation and relationship with geomagnetic activity, *Geophys. Res. Lett.*, *38*, L17107, doi:10.1029/2011GL048671.